

# An artificial neural network model in predicting VTEC over Central Anatolia in Turkey

Ali Özkan

4 Osmaniye Korkut Ata University, Osmaniye Vocational School, 80000, Osmaniye,  
5 Turkey

<sup>6</sup> E-mail address: aliozkan@osmaniye.edu.tr

## Abstract

In this research, the capability of the artificial neural networks to predict GPS VTEC has been investigated over Central Anatolia in Turkey. The VTEC dataset was derived from the 19 permanent GPS stations belonging to TUSAGA-Aktif and IGS networks in the region. The study region extends in the area from west to east bounded by longitudes of  $36.2^{\circ}\text{E}$ - $37.5^{\circ}\text{E}$  and from south to north bounded by latitudes of  $36.0^{\circ}\text{N}$ - $42.0^{\circ}\text{N}$ . Considering the factors inducing VTEC variations in the ionosphere, an artificial neural network was herein proposed that has seven input neurons in a multi-layer perceptron model. The KURU and ANMU permanent GPS stations from TUSAGA-Aktif network were selected to implement the neural network model proposed. Based on the RMSE results achieved in the simulation tests with 50 attempts, the hidden layer in the NN model was designed to have 37 neurons since the lowest RMSE was reached in this attempt. According to the correlation coefficients, absolute and relative errors in the proposed neural network model, the NN VTEC are quite well predicted in hourly and seasonal basis referring to the GPS VTEC. In addition, this paper demonstrated that the NN VTEC model provides better performance than the global IRI model presents. The selected GPS stations, ANMU and KURU, in our GPS network demonstrate well-fitting with the proposed NN to assist the improvement of regional models.

**Keywords:** GPS, Total Electron Content, GPS VTEC, Artificial Neural Network

## 1. Introduction

<sup>28</sup> The ionospheric variations occurring within upper Earth's atmosphere is a

29 complicated phenomena caused by solar activity such as flares and CMEs (Coronal  
30 Mass Ejections). Since the ionosphere has a dispersive feature, electromagnetic  
31 transmissions such as GPS (Global Positioning System) signals propagating through  
32 the ionosphere are exposed to delay. This delay is directly proportional to the TEC  
33 (Total Electron Content) of the ionosphere along the path of the signal. It is described  
34 that TEC is the total number of free electrons in a one-meter squared column  
35 projected along the signal path between the source on the satellite and the receiver on  
36 the Earth [1–3]. The unit of TEC is defined as TECU which equals to  $10^{16}$   
37 electrons/m<sup>2</sup> [3–7]. The slant path with respect to the local vertical at the position of  
38 GPS receiver extends to the satellite as a function of elevation angle. The STEC (slant  
39 TEC) calculated along the path of the GPS signal can be projected into the VTEC  
40 (vertical TEC) by using mapping function [5,8]. VTEC values vary from several to  
41 hundreds TECU due to solar cycle, geographical latitude and longitude, diurnal  
42 variations, seasonal variations, geomagnetic effects and seismic activities [9,10].

43 Besides, global ionospheric models distributed by several organizations such as IGS  
44 CODE (International GNSS Service, Centre for Orbit Determination in Europe), ESA  
45 (European Space Agency), JPL (Jet Propulsion Laboratory), IRI (International  
46 Reference Ionosphere) can also be alternative by interpolating TEC data nearest to the  
47 corresponding position of the GPS receiver [5,11–14].

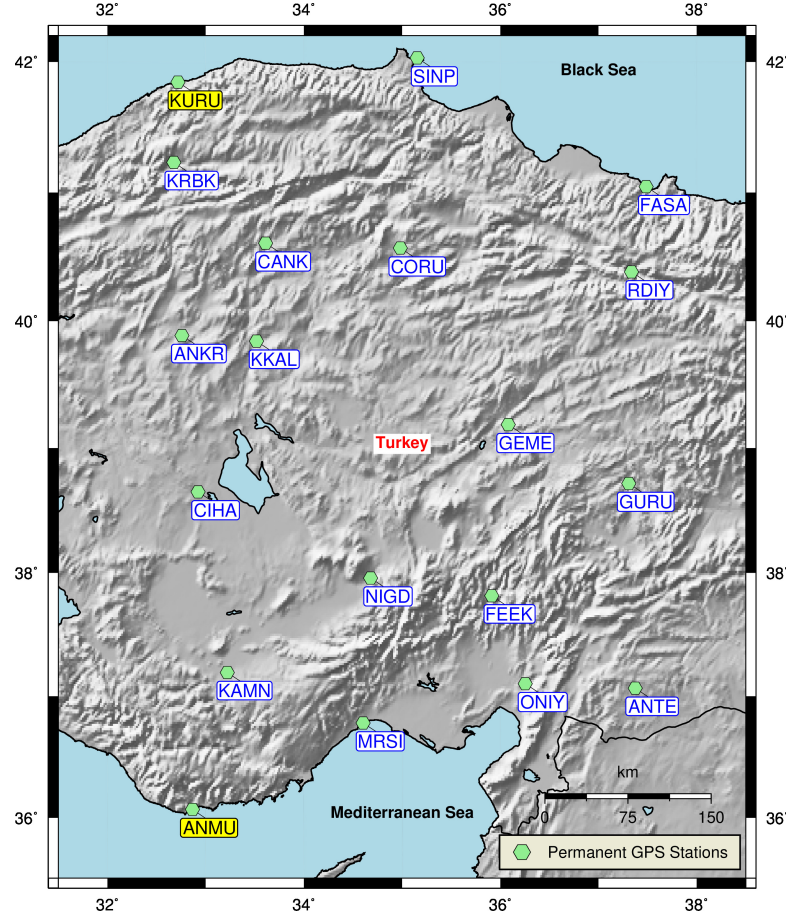
48 Since both the GPS receivers on the ground are sparse to model regional grid of TEC  
49 and also global TEC models have limited accuracy, artificial neural networks are  
50 preferred for predictive modeling of ionosphere [15–19]. Not only ionospheric  
51 variations but also mean temperature predictions [20], solar radiation forecasting [21],  
52 meteorological predictions [22] or tropospheric estimations [23] were recently studied  
53 using neural network models to better interpret the geophysical processes over the  
54 Earth. On the other hand, the spatial and time-dependent components of the  
55 ionospheric activity need to be considered to predict VTEC variations in high spatial  
56 and temporal accuracy [18, 24, 25]. Okoh et al. [18], Homam [24] and Mallika et al.  
57 [25] investigated the neural network performances in terms of VTEC predictions  
58 associated with the spatio-temporal contributors over Equatorial Region. Homam [24]  
59 adopted a data acquisition methodology related to the occurrence of ionospheric  
60 scintillation over a GPS station in Malaysia in order to integrate into neural network  
61 modeling for VTEC predictions. Okoh et al. [18] argued about the effectiveness of the

62 foF2 storm model derived from IRI products, in which it was used as an additional  
63 neuron for the neural input layer in their study over Nigeria. Mallika et al. [25]  
64 investigated the performance of the neural networks in predicting VTEC variations  
65 over India using dense global dataset of IRI models, but with limited ground-based  
66 observations for neural network training and model testing. In this study, it is aimed  
67 to predict significant GPS VTEC based on artificial neural network modeling using  
68 dense ground-based observations obtained from permanent GPS stations within a  
69 regional subnetwork over Central Anatolia in Turkey. The neural network model  
70 proposed here depends on an approach, which contains network training by using a  
71 bulk of GPS data acquired from 19 permanent stations for the period of 2015-2019  
72 and validation of NN VTEC predictions in 2020 with respect to the GPS VTEC and  
73 IRI2012 VTEC at the two northernmost and southernmost GPS stations, KURU and  
74 ANMU, in the mid-latitude region.

75 **2. Materials and methods**

76 *2.1. GPS dataset and analysis*

77 GPS data processed within the scope of this study were obtained from the TUSAGA-  
78 Aktif (Turkish National Permanent GPS Network-Active) and IGS networks over  
79 Central Anatolia in Turkey (Figure 1). The RINEX (Receiver Independent Exchange  
80 Format) files with 30 seconds measurement interval in the 24 hours of observation  
81 span were downloaded from the IGS [26] and TUSAGA-Aktif [27] websites. The  
82 GPS network consisting of 19 permanent stations covers an area from 36.2°E to  
83 37.5°E in longitudes and 36.0°N to 42.0°N in latitudes. Supplementary Table S1  
84 summarizes the detailed descriptions about the permanent GPS stations. The GPS  
85 dataset was generated by selecting specific daily GPS observations in the range of  
86 years for 2015-2020.



87

88 **Figure 1.** GPS network at the central region of Turkey used in this study.

89 In order to derive the total electron content at the locations of permanent stations,  
90 GPS data were processed using the GPS-TEC analysis (Ver. 3.0) software developed  
91 by Gopi Krishna Seemala [28]. The software calculates STEC along the slant  
92 trajectory. The STEC along the slant trajectory can be extracted from the geometry-  
93 free linear combination of GPS observations as per following Eq. (1) [29]:

$$94 \quad STEC = \frac{f_1^2 \cdot f_2^2}{40.3082 \frac{m^3}{s^2} \cdot (f_1^2 - f_2^2)} \{ (P_2 - P_1) - (b_P^s + b_P^r) \} \quad (1)$$

95 where;  $P_1$  and  $P_2$  are pseudorange observables corresponding to the high ( $f_1=1575.42$   
96 MHz) and low ( $f_2=1227.6$  MHz) GPS frequencies respectively,  $b_P^s$  is the pseudorange  
97 satellite delay and  $b_P^r$  is the pseudorange receiver delay. However, the STEC must be  
98 then converted to the VTEC considering a spherical thin-shell model for the  
99 ionosphere. According to the SLM (single layer model), a very thin layer at a fixed  
100 height above the Earth's surface contains all the free electrons [6].

101 Thus, as given in following equations, VTEC at ionospheric pierce point is derived

102 using a mapping function [7,30,31] based on the SLM:

103 
$$STEC = VTEC \cdot M(z) + (b_s + b_r + b_{rx}) \quad (2)$$

104 with

105 
$$M(z) = \frac{1}{\cos z^1} = \frac{1}{\sqrt{1 - \sin^2 z^1}} \quad (3)$$

106 
$$\sin z^1 = \frac{R}{R+H} \cdot \sin z \quad (4)$$

107 where;  $M(z)$  is the mapping function,  $R$  is the Earth's mean radius,  $b_s$  is satellite bias,  
108  $b_r$  is receiver bias,  $b_{rx}$  is receiver interchannel bias,  $H$  is the ionospheric layer height,  $z$   
109 and  $z'$  are the zenith angles at the receiver site and at the ionospheric pierce point,  
110 respectively. In this study, the ionospheric layer was assumed at a fixed height of 350  
111 km above the Earth's surface. In addition, the sampling rate of each GPS receiver was  
112 30 seconds and the minimum elevation angle criterion was assumed to be 30° in case  
113 any multipath effects might distort the GPS observations.

114 *2.2. Artificial Neural Network Approach*

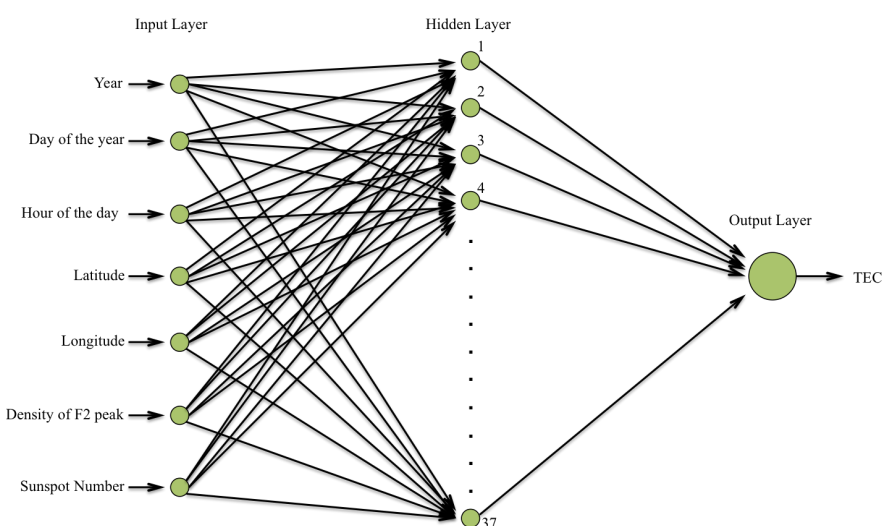
115 Neural networks are regarded as artificial intelligence mechanisms that can be trained  
116 and are able to learn to deal with non-linear input/output relationships in the  
117 complicated processes [32,33]. The mechanism contains simple processing elements  
118 named as artificial neurons, in which the summation provided by manipulating the  
119 input signal using weights is stored. The determination of the weights of the input  
120 signal in an artificial neural network is realized by an iterative adjustment procedure  
121 during the training process until the optimum weights are achieved [34]. Once the  
122 neural network is trained, the input signal passes through an activation function  
123 (transfer function) to generate output of neurons. Sigmoid activation function given in  
124 Eq. (5) is usually preferred as activation function in multi-layer perceptron model.

125 
$$f(x) = \frac{1}{1 + e^{-x}} \quad (5)$$

126 The activation function serves as non-linear filter to generate output signal. During  
127 the training stage, a back-propagation algorithm is applied in feed-forward and feed-  
128 backward processes. In an iterative approach, the biases of the neural network are  
129 adjusted repeatedly until the RMSE (root mean square error) reaches a threshold  
130 value for the output signal. In this study, the activation function of all layers is the

131 sigmoid function and Levenberg-Marquardt back-propagation algorithm was applied  
132 to train the network.

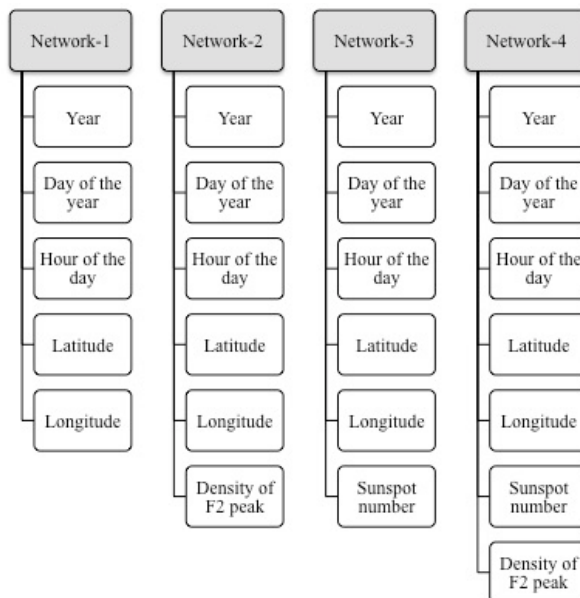
133 Due to its quick response for predictions and effectiveness during training process, the  
134 multi-layer perceptron neural network consisting of one input layer, one hidden layer  
135 with many neurons and one output layer was preferred in this study. The optimal  
136 number of neurons and layers can be decided in consequence of trial and error as per  
137 each specific problem [35]. The strategy followed here to determine the optimal  
138 number of neurons in hidden layer was realized using different neural network  
139 designs with varying input neurons. Since VTEC is associated with the solar cycle  
140 variations, seasonal variations, diurnal variations, spatial variations and solar activity  
141 variations, the proposed neural network herein was anticipated to learn considering  
142 those parameters. The data about the sunspot numbers were provided from the  
143 website of World Data Center Sunspot Index and Long-term Solar Observations [36].  
144 Additionally, the relationship between VTEC and electron density at F2 peak ( $NmF2$ )  
145 has a strong positive correlation [37,38] so that the learning stage of the network was  
146 considered to be more effective by incorporation of the  $NmF2$  data obtained from the  
147 IRI model [39]. Furthermore, the IRI is an empirical ionospheric model that  
148 introduces reliable global data accompanying with long-term solar cycle variations  
149 [18]. Accordingly, the input layer of our neural network contains seven neurons  
150 namely year, day of the year, hour of the day, latitude, longitude, sunspot number and  
151 electron density at F2 peak (Figure 2).



152

153 **Figure 2.** The structure of the multi-layer perceptron neural network with one  
154 hidden layer used in this research.

155 Using the different combinations of input neurons, several network designs were  
156 statistically tested for the determination of the optimal architecture of the neural  
157 network. The different neural networks were designed from the simplest structure to  
158 more complex one, in which varying parameters and numbers of input neurons were  
159 considered (Figure 3).



160

161 **Figure 3.** The different neural network designs with the corresponding input  
162 neurons in each.

163 Considering a test procedure to determine which network design was the most  
164 appropriate for network training, each of four network designs was simulated 50 times  
165 in terms of varying numbers of neurons in the hidden layer. The decision criterion of  
166 the testing procedure was the RMSE parameter statistically expected to be the lowest  
167 based on the predictions in the neural networks [40].

168 The analyses within this research covers the period between 2015 and 2020. The  
169 strategy to constitute a dataset was adopted by selecting the days with the weakest  
170 ionospheric activity for each month. Hourly-averaged VTEC values calculated from  
171 GPS observations were the output signal of the neural network. It is worth to say that  
172 the training dataset differs from the dataset used in the random model testing. In the  
173 random testing, the proposed model has been assessed in terms of the temporal  
174 performance. The dataset for the period of 2015-2019 was acquired from all the  
175 permanent stations performing in the GPS network demonstrated in Suppl. Figure 1  
176 and allocated to training by 70% of it, validation by 15% of it and testing by 15% as

of remaining. This training dataset was randomly selected among the daily GPS data acquired in those permanent GPS stations during the weakest day of each month in a year, which means that each station provides data of 4 out of 12 random weakest days in a year. Apart from this dataset used to train the neural network, the GPS data for the year of 2020 acquired from KURU ( $41.846^{\circ}\text{N}$ ,  $32.718^{\circ}\text{E}$ ) and ANMU ( $36.069^{\circ}\text{N}$ ,  $32.865^{\circ}\text{E}$ ) permanent stations were randomly used to test the neural network model. There were two criteria for the data selection in random testing stage, as one of them was to use the data out of the training dataset period, which were 2020 GPS data here and the other was choosing the northernmost and the southernmost stations to notice the spatial variations. In addition, the diurnal performance of the neural network was tested for different times of a day namely 03:00 UTC (Coordinated Universal Time) equivalent to 06:00 Local Time, 09:00 UTC (12:00 Local Time), 15:00 UTC (18:00 Local Time) and 21:00 UTC (00:00 Local Time), which correspond to near the time of sunrise, the noontime with high ionospheric level, near the time of sunset and the midnight, respectively. Besides, in order to test the seasonal performance of the neural network, the predictions were also tested for different seasons in 2020 namely vernal equinox, summer solstice, autumnal equinox and winter solstice.

The performance of our neural network was assessed in terms of the absolute and relative errors estimated using following equations, respectively:

$$|E_{abs}| = |TEC_{NN} - TEC_{GPS}| \quad (6)$$

$$|E_{rel}| = \left( \frac{|E_{abs}|}{TEC_{GPS}} \right) \times 100 \quad (7)$$

where;  $E_{abs}$  is the absolute error,  $E_{rel}$  is the relative error,  $TEC_{NN}$  and  $TEC_{GPS}$  are predicted VTEC by the neural network and GPS-derived VTEC, respectively [19,41]. In this context, the less the absolute and relative errors, the closer the predicted VTEC values by neural network model and calculated VTEC values from GPS observations.

### 202 3. Results and discussions

203 First, in order to determine the optimum architecture of the neural network, all the  
204 proposed neural network designs were compared based on the RMSEs for the dataset  
205 period between 2015 and 2019. In this research, the RMSEs indicating the deviations  
206 of predicted VTEC by the neural network (hereinafter referred to as NN VTEC) from

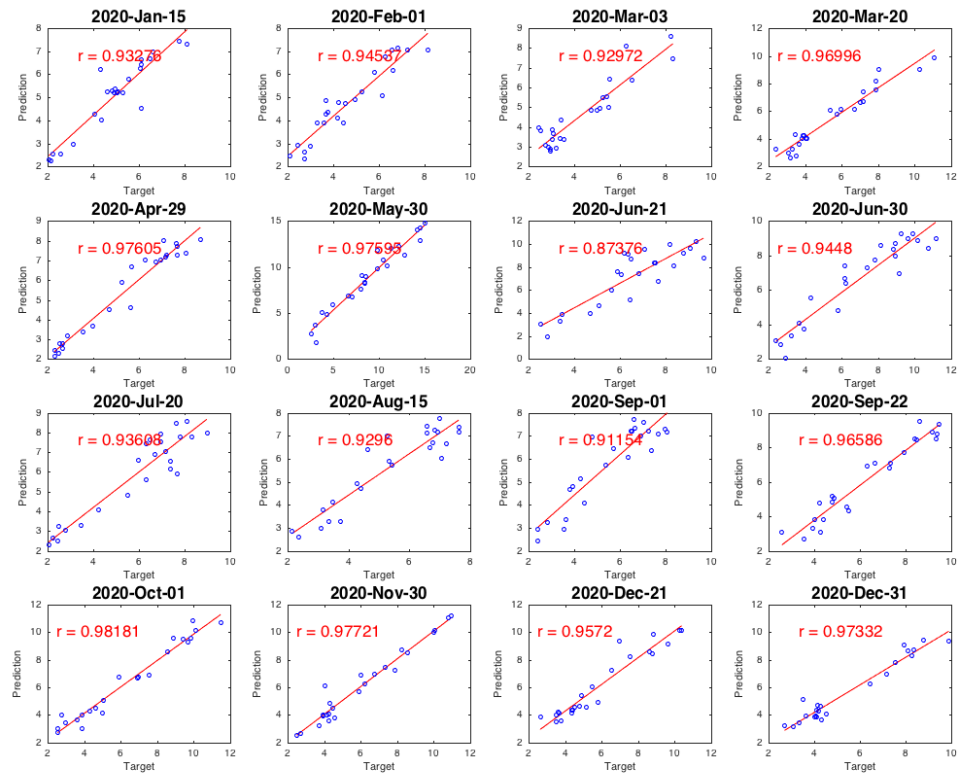
207 observed VTEC by means of GPS (hereinafter referred to as GPS VTEC) were  
208 calculated per the number of neurons in hidden layer for each network designs  
209 individually. Both in Suppl. Figure S1 and Figure S2, it is evidently proven that the  
210 Net4 consisting of seven input neurons namely the year, day of the year, hour of the  
211 day, latitude, longitude, sunspot number, density of F2 peak neurons has the lowest  
212 RMSE compared to other three network designs. The RMSE for the dataset of KURU  
213 and ANMU stations has the minimum value (~1.2 TECU) for the simulation test  
214 using 37 neurons in the hidden layer, which indicates the best agreement between the  
215 NN VTEC and GPS VTEC (Suppl. Figure S2). Thus, the training of the network was  
216 achieved using seven neurons in the input layer and 37 neurons in the hidden layer.

217 Besides, it is clear that the higher the RMSE, the worst the neural network design  
218 performance. The first neural network design (Net1) has the highest RMSEs  
219 compared to other network designs that means the fewer input neurons in, the poorer  
220 the network performance. Furthermore, the second (Net2) and third (Net3) neural  
221 network designs have moderate performances compared to the Net1 (the worst) and  
222 the Net4 (the best). As a result, the increase in the number of input neurons helps the  
223 neural network to learn better and to make more reasonable predictions.

224 In Figure 4 and Figure 5, the NN VTEC (prediction in the vertical axis) versus the  
225 GPS VTEC (target in the horizontal axis) was plotted for KURU and ANMU stations  
226 for the 2020 dataset, respectively. The scatter plots for the predictions and their  
227 corresponding targets demonstrate the red lines of best fitting for regression model  
228 together with the correlation coefficients ( $r$ ). It is a fact that there is a high correlation  
229 between NN VTEC and GPS VTEC since all the correlation coefficients except the  
230 lowest two are above 0.9 for both KURU and ANMU stations. The lowest correlation  
231 coefficients were 0.87376 for KURU station in June 21, 2020 and 0.84408 for ANMU  
232 station in July 20, 2020.

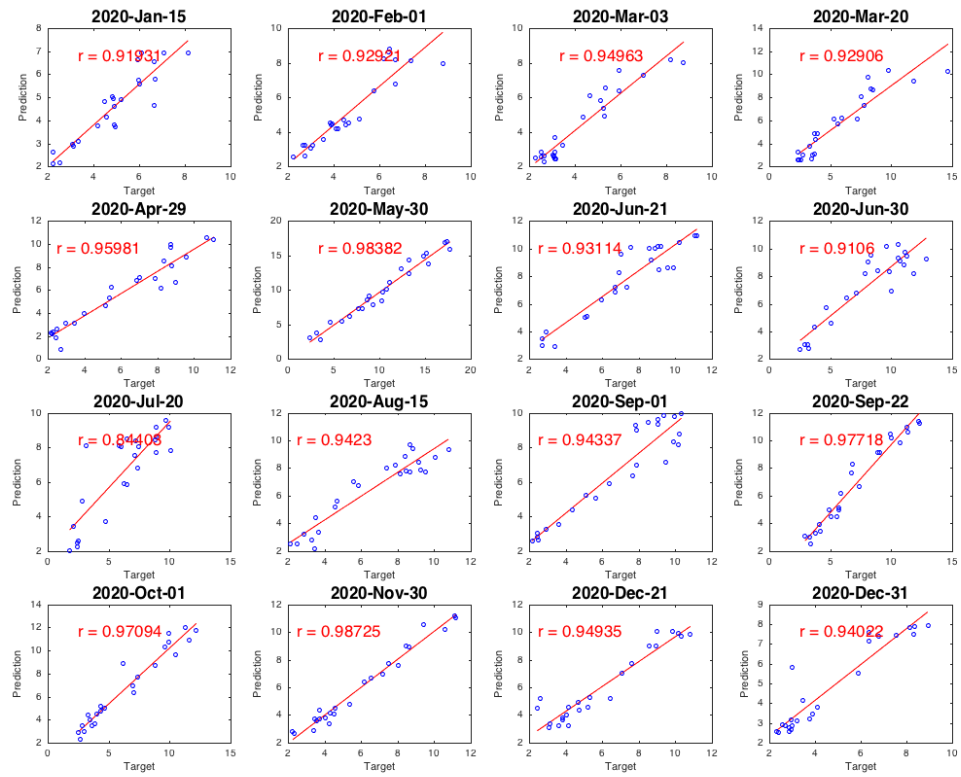
233

234 **Figure 4.** The correlations between the NN VTEC and the GPS VTEC for the 2020  
 235 dataset over KURU station.



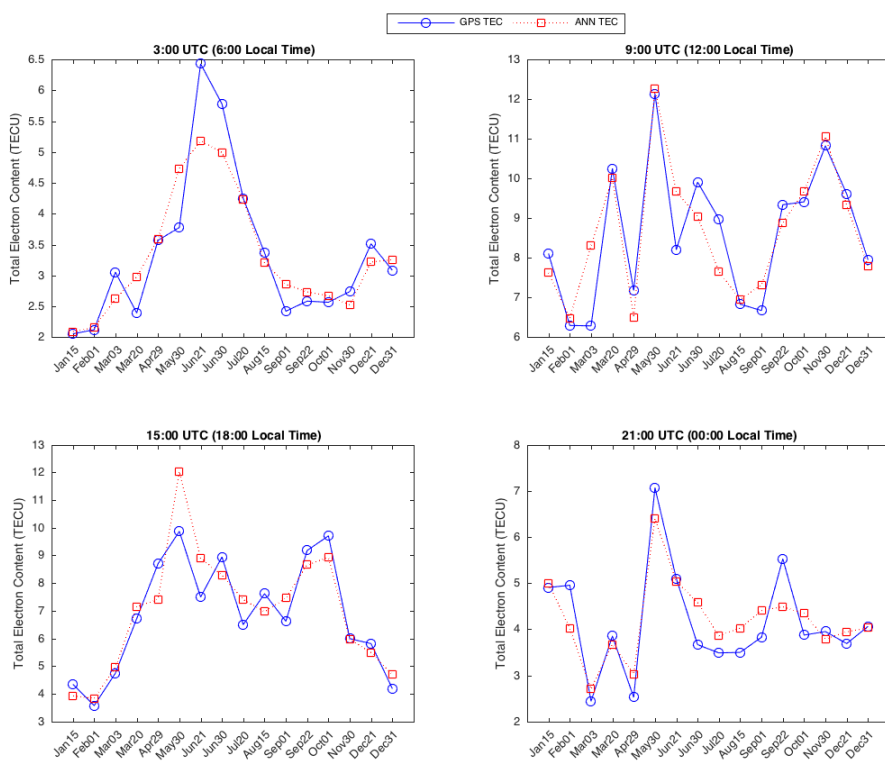
236

237 **Figure 5.** The correlations between the NN VTEC and the GPS VTEC for the 2020  
 238 dataset over ANMU station.



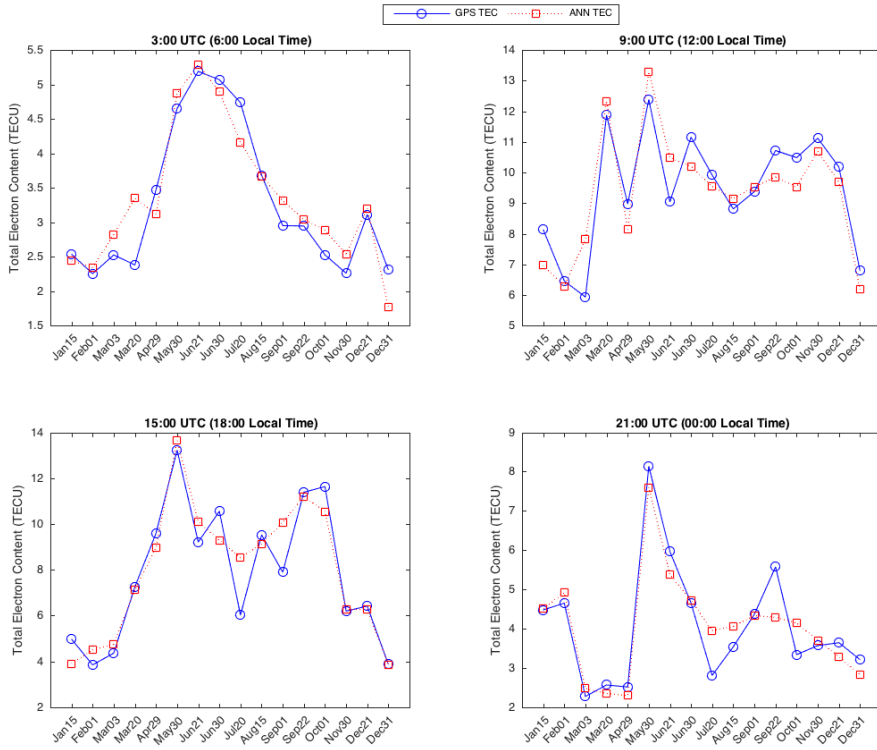
239 In order to evaluate the diurnal performance of the neural network, NN VTEC was  
 240 compared with the corresponding GPS VTEC for the specific times of the day during  
 241 2020 over KURU and ANMU stations. These times within the day were determined  
 242 based on the positions of the sun with respect to the local during the day as the near  
 243 the time of sunrise, the noontime with high ionospheric level, near the time of sunset  
 244 and the midnight. Thus, 03:00 UTC (06:00 Local Time), 09:00 UTC (12:00 Local  
 245 Time), 15:00 UTC (18:00 Local Time) and 21:00 UTC (00:00 Local Time) were  
 246 considered as the benchmarks for intraday variations. The local time in Turkey is 3  
 247 hours ahead of the universal time.

248 The NN VTEC obtained from the neural network model and GPS VTEC calculated  
 249 from the GPS observations were compared in hourly basis for those specific times of  
 250 the day during 2020 over KURU and ANMU stations (Figure 6 and Figure 7).  
 251 Additionally, the absolute and relative errors of NN VTEC from GPS VTEC for those  
 252 specific times of the day during 2020 over KURU and ANMU stations were  
 253 demonstrated, respectively, in Supplementary Figure S3-S6. From those figures, it is  
 254 evident that the predictions (NN VTEC) for the specific times of the day during 2020  
 255 are highly correlated with the targets (GPS VTEC) since the highest absolute errors  
 256 does not exceed the value of 2.5 TECU during 2020 over both stations.



257

258 **Figure 6.** Hourly comparison of NN VTEC and GPS VTEC over KURU station.



259

260

**Figure 7.** Hourly comparison of NN VTEC and GPS VTEC over ANMU station.

261

**Table 1.** The correlation coefficients for the comparison of the specific day times

| Station | 03:00 UTC | 09:00 UTC | 15:00 UTC | 21:00 UTC |
|---------|-----------|-----------|-----------|-----------|
| KURU    | 0.91149   | 0.87642   | 0.85907   | 0.91008   |
| ANMU    | 0.93391   | 0.89154   | 0.93463   | 0.92716   |

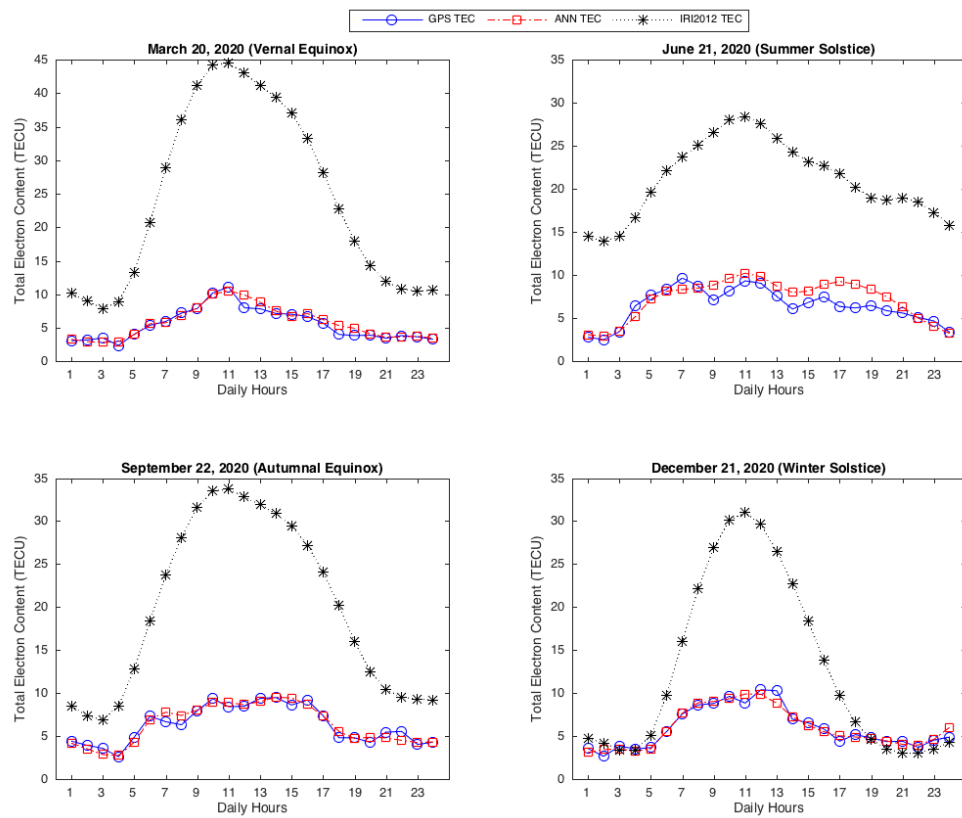
262

As seen from the plots in Figure 6 and Figure 7, the NN VTEC and GPS VTEC at all day times over both KURU and ANMU stations have mostly similar trends during 2020 indicating good predictions for the GPS VTEC. The NN VTEC and GPS VTEC indicate the goodness of fitting with the correlation coefficient of more than 0.85 for different day times over KURU and ANMU stations (Table 1). In Supplementary Figure S3 and Figure S4, it is noticed that the absolute errors over those stations are less than 2.5 TECU throughout the year. Accordingly, the maximum relative errors are less than the limits of 35% and 45% over KURU and ANMU stations, respectively (Suppl. Figure S5 and Figure S6).

271

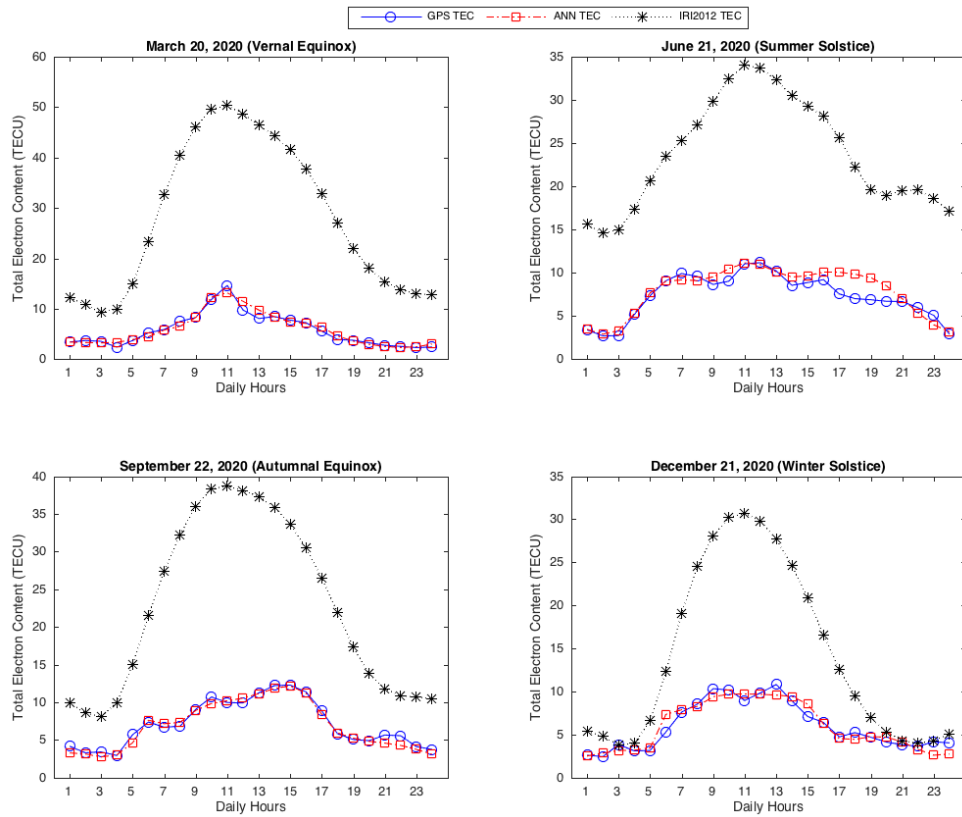
On the other hand, another perspective in evaluating the performance of the neural network is based on the seasonal variations of VTEC. Thus, the different seasons in 2020 namely vernal equinox, summer solstice, autumnal equinox and winter solstice were considered to investigate the seasonal variations. In the seasonal evaluation

process, the IRI2012 VTEC derived from IRI2012 model using NeQuick parameter for the Ne topside was also incorporated into the analysis in order to compare the neural network model with an international reference model. Accordingly, the seasonal comparison of the NN VTEC with the GPS VTEC and the IRI2012 VTEC was demonstrated in Figure 8 and Figure 9. As also seen from the correlation coefficients, it is very clear that the NN VTEC provides much better correlation with the GPS VTEC than the IRI2012 VTEC has (Table 2).



282

283 **Figure 8.** The seasonal comparison of the NN VTEC and the IRI2012 VTEC with  
284 the GPS VTEC during 2020 over KURU station.



285

286 **Figure 9.** The seasonal comparison of the NN VTEC and the IRI2012 VTEC with  
 287 the GPS VTEC during 2020 over ANMU station.

288

**Table 2.** The correlation coefficients for the comparison of seasonal variations.

| Station Code | Model        | Vernal Equinox (March 20) | Summer Solstice (June 21) | Autumnal Equinox (September 22) | Winter Solstice (December 21) |
|--------------|--------------|---------------------------|---------------------------|---------------------------------|-------------------------------|
| KURU         | NN VTEC      | 0.95349                   | 0.92844                   | 0.96560                         | 0.96070                       |
|              | IRI2012 VTEC | 0.94893                   | 0.85616                   | 0.91466                         | 0.94949                       |
| ANMU         | NN VTEC      | 0.97437                   | 0.92746                   | 0.98680                         | 0.95510                       |
|              | IRI2012 VTEC | 0.91737                   | 0.90834                   | 0.91173                         | 0.96866                       |

289

#### 4. Conclusions

290 The GPS data obtained from the TUSAGA-Aktif and IGS networks over the Central  
 291 Anatolia in Turkey was used as the output of this research. The GPS network  
 292 consisting of 19 permanent stations provided also random data for the training of the  
 293 neural network. The neural network structure was established using the seven input

neurons namely year, day of the year, hour of the day, latitude, longitude, sunspot number and electron density at F2 peak. The optimal numbers of the input neurons and the neurons in the hidden layer were determined as per the simulation tests aimed to reach the lowest RMSE. The neural network design with seven input neurons (Net4) verified the lowest RMSE compared to the other network designs. The simulation tests demonstrated that the more input neurons integrated into the input layer, the better the network training and the more significant the predictions. Additionally, the target GPS dataset for the neural network model has here played pivotal role. Unlike the targets used in the network training, it was aimed to achieve a network validation process using unique independent targets in the model testing. Thus, the target dataset was divided into two categories. The one for network training contains random GPS data acquired from 19 permanent stations during the period of 2015-2019. On the contrary, the model testing was accomplished by using a different bulk of targets calculated from the GPS observations in 2020. From this perspective, some significant indicators prove the applicability of the proposed model such that the correlations between the predictions for the NN VTEC and their corresponding targets for GPS VTEC have pointed out quite well fitting at the selected days in 2020. Those selected days were determined as per the weakest ionospheric activity within each month during the year. Using this multi-layer perceptron model, the diurnal variations of VTEC can be predicted quite well by the proposed neural network structure at the specific day times since the absolute and relative errors in TECU are very low. The correlation coefficients also simply demonstrate well fitting for diurnal predictions, indicating that the different day times are not deterrent in the modeling. Considering the correlation coefficients and the absolute errors of the NN VTEC from the GPS VTEC, the seasonal comparison of the NN VTEC with the GPS VTEC notices the high accurate prediction capability of the neural network model during different seasons in 2020. During equinox seasons, the ANMU station evidently demonstrates better in fitting with the proposed neural network while the KURU station outperforms during summer and winter solstices. As also expected, during the all seasons in 2020, the NN VTEC provides better predictions for the seasonal variations than the IRI2012 VTEC obtained from the global IRI model. To conclude, instead of competing with the global models like IRI, the proposed model in this study is there to elaborate the power of such neural network models in predicting the VTEC since those models could be a well contributor to improve the regional models.

328    **Declaration of Competing Interest**

329    The author declares that he has no known competing financial interests or personal  
330    relationships that could have appeared to influence the work reported in this paper.

331    **References**

- 332    [1]    Y. Huang, K. Cheng, S. Chen, On the equatorial anomaly of the ionospheric  
333    total electron content near the northern anomaly crest region, *Journal of*  
334    *Geophysical Research: Space Physics*. 94 (1989) 13515–13525.
- 335    [2]    R.G. Rastogi, J.A. Klobuchar, Ionospheric electron content within the  
336    equatorial F 2 layer anomaly belt, *Journal of Geophysical Research: Space*  
337    *Physics*. 95 (1990) 19045–19052.
- 338    [3]    B. Hofmann-Wellenhof, H. Lichtenegger, J. Collins, Global positioning  
339    system: theory and practice, Springer Science & Business Media, 2012.
- 340    [4]    G. Seeber, Satellite Geodesy: Foundations, Methods and Applications,  
341    *International Hydrographic Review*. 4 (2003) 92–93.
- 342    [5]    S. Schaer, Mapping and predicting the Earth's ionosphere using the Global  
343    Positioning System, Ph.D. Thesis, Astronomical Institute, University of Bern.  
344    (1999).
- 345    [6]    U. Wild, Ionosphere and geodetic satellite systems: permanent GPS tracking  
346    data for modelling and monitoring., *Geod.-Geophys. Arb. Schweiz.* 48 (1994).
- 347    [7]    A.J. Mannucci, B.D. Wilson, C.D. Edwards, A New Method for Monitoring  
348    the Earth's Ionospheric Total Electron Content Using the GPS Global Network,  
349    in: Proceedings of the 6th International Technical Meeting of the Satellite  
350    Division of The Institute of Navigation (ION GPS 1993), 1993: pp. 1323–  
351    1332.
- 352    [8]    J.S. Shim, Analysis of total electron content (TEC) variations in the low-and  
353    middle-latitude ionosphere, Ph.D. Thesis. (2009).
- 354    [9]    R. Warnant, E. Pottiaux, The increase of the ionospheric activity as measured  
355    by GPS, *Earth, Planets and Space*. 52 (2000) 1055–1060.

- 356 [10] G. Liu, W. Huang, J. Gong, H. Shen, Seasonal variability of GPS-VTEC and  
357 model during low solar activity period (2006-2007) near the equatorial  
358 ionization anomaly crest location in Chinese zone, *Advances in Space*  
359 *Research.* 51 (2013) 366–376. <https://doi.org/10.1016/j.asr.2012.09.002>.
- 360 [11] D. Bilitza, D. Altadill, Y. Zhang, C. Mertens, V. Truhlik, P. Richards, L.-A.  
361 McKinnell, B. Reinisch, The International Reference Ionosphere 2012—a model  
362 of international collaboration, *Journal of Space Weather and Space Climate.* 4  
363 (2014) A07.
- 364 [12] S.K. Leong, T.A. Musa, K. Omar, M.D. Subari, N.B. Pathy, M.F. Asillam,  
365 Assessment of ionosphere models at Banting: Performance of IRI-2007, IRI-  
366 2012 and NeQuick 2 models during the ascending phase of Solar Cycle 24,  
367 *Advances in Space Research.* 55 (2015) 1928–1940.
- 368 [13] R. Scharroo, W.H.F. Smith, A global positioning system-based climatology for  
369 the total electron content in the ionosphere, *Journal of Geophysical Research:*  
370 *Space Physics.* 115 (2010) A10318.
- 371 [14] W. Wan, F. Ding, Z. Ren, M. Zhang, L. Liu, B. Ning, Modeling the global  
372 ionospheric total electron content with empirical orthogonal function analysis,  
373 *Science China Technological Sciences.* 55 (2012) 1161–1168.
- 374 [15] A.J. Coster, J.C. Foster, P.J. Erickson, Monitoring the ionosphere with GPS,  
375 *GPS World.* 14 (2003).
- 376 [16] Z. Liu, Y. Gao, Ionospheric TEC predictions over a local area GPS reference  
377 network, *GPS Solutions.* 8 (2004) 23–29.
- 378 [17] A. Vernon, L.R. Cander, Regional GPS receiver networks for monitoring local  
379 mid-latitude total electron content, *Annals of Geophysics.* 45 (2002) 649–656.
- 380 [18] D. Okoh, O. Owolabi, C. Ekechukwu, O. Polarim, G. Arhiwo, J. Agbo, S.  
381 Bolaji, B. Rabiu, A regional GNSS-VTEC model over Nigeria using neural  
382 networks: A novel approach, *Geodesy and Geodynamics.* 7 (2016) 19–31.
- 383 [19] R.F. Leandro, M.C. Santos, A neural network approach for regional vertical

- 384 total electron content modelling, *Studia Geophysica et Geodaetica*. 51 (2007)  
385 279–292. <https://doi.org/10.1007/s11200-007-0015-6>.
- 386 [20] M. Ding, A neural network model for predicting weighted mean temperature,  
387 *Journal of Geodesy*. 92 (2018) 1187–1198.
- 388 [21] S. Pereira, P. Canhoto, R. Salgado, M.J. Costa, Development of an ANN based  
389 corrective algorithm of the operational ECMWF global horizontal irradiation  
390 forecasts, *Solar Energy*. 185 (2019) 387–405.
- 391 [22] A. Manzato, A. Pucillo, A. Cicogna, Improving ECMWF-based 6-hours  
392 maximum rain using instability indices and neural networks, *Atmospheric  
393 Research*. 217 (2019) 184–197.
- 394 [23] M.O. Selbesoglu, Prediction of tropospheric wet delay by an artificial neural  
395 network model based on meteorological and GNSS data, *Engineering Science  
396 and Technology, an International Journal*. 23 (2020) 967–972.
- 397 [24] M.J. Homam, Prediction of total electron content of the ionosphere using  
398 neural network, *Jurnal Teknologi*. 78 (2016).
- 399 [25] L. Mallika I, D.V. Ratnam, S. Raman, G. Sivavaraprasad, Performance analysis  
400 of Neural Networks with IRI-2016 and IRI-2012 models over Indian low-  
401 latitude GPS stations, *Astrophysics and Space Science*. 365 (2020) 1–14.
- 402 [26] URL-1, International GNSS Service, (n.d.). <https://igs.org/> (accessed January  
403 31, 2022).
- 404 [27] URL-2, TUSAGA-Aktif, (n.d.). <https://www.tusaga-aktif.gov.tr/> (accessed  
405 January 31, 2022).
- 406 [28] URL-3, GPS-TEC analysis software, (n.d.). <http://seemala.blogspot.com>  
407 (accessed January 31, 2022).
- 408 [29] M.A. Sharifi, S. Farzaneh, Local Ionospheric Modeling Using the Localized  
409 Global Ionospheric Map and Terrestrial GPS, *Acta Geophysica*. 64 (2016)  
410 237–252.

- 411 [30] Y. Norsuzila, M. Abdullah, M. Ismail, Leveling Process of Total Electron  
412 Content(TEC) Using Malaysian Global Positioning System(GPS) Data,  
413 American Journal of Engineering and Applied Sciences. 1 (2008).
- 414 [31] Y. Xiang, Y. Gao, An enhanced mapping function with ionospheric varying  
415 height, Remote Sensing. 11 (2019) 1497.
- 416 [32] L.R. Cander, M.M. Milosavljevic, S.S. Stankovic, S. Tomasevic, Ionospheric  
417 forecasting technique by artificial neural network, Electronics Letters. 34  
418 (1998) 1573–1574.
- 419 [33] R.F. Leandro, M.C. Santos, Comparison between autoregressive model and  
420 neural network for forecasting space environment parameters, Bollettino Di  
421 Geodesia e Scienze Affini. 63 (2004) 197–212.
- 422 [34] T. Kohonen, Adaptive, associative, and self-organizing functions in neural  
423 computing, Applied Optics. 26 (1987) 4910–4918.
- 424 [35] P.K. Simpson, Artificial Neural Systems: Foundations Paradigms, Pergamon  
425 Press, New York, 1990.
- 426 [36] URL-5, World Data Center SILSO, (n.d.). <https://wwwbis.sidc.be/silso/>  
427 (accessed January 31, 2022).
- 428 [37] H. Jin, T. Maruyama, 3-3-2 Different behaviors of TEC and NmF2 observed  
429 during large geomagnetic storms, Journal of the National Institute of  
430 Information and Communications Technology Vol. 56 (2009).
- 431 [38] R. Leitinger, L. Ciraolo, L. Kersley, S.S. Kouris, P. Spalla, Relations between  
432 electron contentand peak density: regular and extreme behaviour, Annals of  
433 Geophysics. 47 (2004).
- 434 [39] URL-4, Community Coordinated Modeling Center (CCMC), (n.d.).  
435 <https://ccmc.gsfc.nasa.gov> (accessed January 31, 2022).
- 436 [40] A.J. Conway, K.P. Macpherson, G. Blacklaw, J.C. Brown, A neural network  
437 prediction of solar cycle 23, Journal of Geophysical Research: Space Physics.  
438 103 (1998) 29733–29742.

439 [41] M.R.G. Razin, B. Voosoghi, A. Mohammadzadeh, Efficiency of artificial  
440 neural networks in map of total electron content over Iran, *Acta Geodaetica et*  
441 *Geophysica.* 51 (2016) 541–555. <https://doi.org/10.1007/s40328-015-0143-3>.

442 **Supplementary Material Link:**

443 [https://github.com/aliozk4n/Supplementary\\_Material.git](https://github.com/aliozk4n/Supplementary_Material.git)